

LETTER

Photo-induced charge density distribution in metal surfaces and its extraction with apertureless near-field optics

To cite this article: S T Chui *et al* 2019 *J. Phys.: Condens. Matter* **31** 24LT01

View the [article online](#) for updates and enhancements.



IOP | ebooks™

Bringing you innovative digital publishing with leading voices to create your essential collection of books in STEM research.

Start exploring the **collection** - download the first chapter of every title for free.

Letter

Photo-induced charge density distribution in metal surfaces and its extraction with apertureless near-field optics

S T Chui¹, Xinzhong Chen², Hai Hu³, Debo Hu³, Qing Dai³
and Mengkun Liu²

¹ Bartol Research Institute and Department of Physics and Astronomy, University of Delaware, Newark, DE 19716, United States of America

² Department of Physics and Astronomy, Stony Brook University, Stony Brook, NY 11794, United States of America

³ Division of Nanophotonics, CAS Center for Excellence in Nanoscience, National Center for Nanoscience and Technology, Beijing 100190, People's Republic of China

E-mail: chui@udel.edu

Received 21 December 2018, revised 10 March 2019

Accepted for publication 14 March 2019

Published 2 April 2019



Abstract

Electromagnetic (EM) waves impinging on finite metallic structures can induce non-uniform electrical currents and create oscillating charge densities. These local charges govern the important physical processes such as plasmonic behavior or enhanced Raman scattering. Yet the quantitative calculation and probing of the spatial distribution of the charge density still remain challenging at the subwavelength scale. This is especially the case if one considers the boundary effect, where the charge density can become divergent and conventional finite element methods fail to obtain accurate information. With an approach we recently developed, we calculate this charge density for subwavelength structures with and without sharp corners: gold disks and equilateral triangles. We also devise an independent way to extract the surface charge density distributions from experiments using scattering-type scanning near-field optical microscope (s-SNOM). We found that the charge density σ is related to the near field signal S_n by $\sigma_{\text{element}} \propto (S_n - \langle S_n \rangle) / \langle S_n \rangle$. With no adjustable parameters, the extracted surface charge distribution from the experiments matches well with that from the theoretical prediction, both in magnitude and phase. Our work provides a quantitative study of the surface charge distributions and a systematic and rigorous treatment to extract surface charge distributions at the nanoscale, opening opportunities for mining the near-field data from s-SNOM.

Keywords: s-SNOM, charge density, scattering

(Some figures may appear in colour only in the online journal)

An external electromagnetic (EM) wave excites charge currents which are particularly significant for metallic surfaces. The currents are generally spatially nonuniform and therefore lead to charge density oscillation at the same frequency as the incident field. This local charge density distribution determines the behavior of a wide variety of surface phenomena

such as interface polariton transport, plasmonic field enhancement, and nanoscale surface-enhanced Raman scattering [1]. However, it is difficult to obtain accurate information of these photo-induced charges with conventional finite element methods, especially for subwavelength objects with sharp boundaries.

In this paper, we address this problem both theoretically and experimentally and illustrate our ideas with the examples of subwavelength metal disks and metal triangles under external light illumination. In particular, using an approach we recently developed [2, 3], we obtain theoretically the charge densities induced by infrared light on subwavelength-sized metallic disks and equilateral triangles. For the disks, we find that the induced charge density is a sum of a bulk term and an edge term, with the latter localized near the circular perimeter of the disk. This differs from the results obtained in the case of electrostatics where the net current is zero inside the metallic element and all the charges are localized at the boundaries. For the triangles, we calculate the amplitude and phase of the induced charges and find charges with different signs at different corners. Experimentally, we devise a way to extract the charge distribution from near-field optical signals mapped with s-SNOM [4, 5]. With no adjustable parameters, the extracted surface charge distribution from the experiments matches well with that from the theoretical prediction.

Our results for the metallic structures with and without corners provide support that the local charge densities can be extracted for general metamaterial structures using s-SNOM data. We first discuss the calculation for the case of a metallic disk with radius R in an external EM field. This is based on our recently developed rigorous first-principles circuit element method [2]. In our formulation, the physical quantities are expressed not in a mesh but in terms of a complete orthonormal set of basis functions. The current density \mathbf{j} is related to the external electric field \mathbf{E}_{ext} by a circuit equation in terms of an impedance matrix \mathbf{Z} which is just a representation of the Green's function in our basis⁴:

$$\mathbf{j} = \mathbf{Z}^{-1}(\mathbf{E}_{\text{ext}} + \mathbf{E}^s). \quad (1)$$

\mathbf{E}^s is the field at the tip determined from the condition that the current induced by the external field outside of the tip is zero. Our approach provides a good physical understanding of the problem and is orders of magnitude faster than current numerical approaches. From charge current conservation, the charge density σ/t for a film of thickness t is related to the current density as $\sigma = t\nabla \cdot \mathbf{j}/(i\omega)$. We find that the surface charge density σ is a sum of a bulk term and an edge term localized near the circular perimeter of the disk. The bulk surface charge density is approximately proportional to $\sigma^{\text{bulk}}(r) \cos \phi$; the edge density, $\delta(r - R) \cos \phi$. In electrostatics, the bulk density inside the disk is zero.

A two dimensional contour plot of the real part of the theoretical bulk charge density distribution of a form $\cos \phi$ is shown in figure 1(b). This is comparable to the results extracted from experimental s-SNOM data in figure 1(a) for a disk of radius $0.53 \mu\text{m}$ and thickness 40 nm under incident light of wavelength $6 \mu\text{m}$. We explain this next.

In s-SNOM [4, 5, 6], an electromagnetic (EM) wave is scattered from both the sample and the vibrating atomic force microscope (AFM) tip on top, as is illustrated in figure 2. The near-field tip-sample interactions with 10 nm spatial resolution

is contained in the scattered field S_n demodulated at the higher harmonics ($n = 2, 3, 4$) of the tapping frequency Ω of the tip. s-SNOM has been employed to investigate a wide variety of phenomena such as mesoscale metal-insulator phase coexistence [7–13] and surface polariton propagation [14–19], and metallic nanostructure-light interactions [20–24].

We recently investigated [25] the scattering of EM waves from the conical tip using an approach we developed [2, 3, 26]⁵. When compared with s-SNOM experimental results for the insulator SiO_2 , our previous calculation provides very good agreement. We found that an external field scatters from the tip and generates currents along it. For example, the experiment described here was carried out at a wavelength of $\lambda = 6 \mu\text{m}$, cone height, base and tip radii of $20 \mu\text{m}$, $5 \mu\text{m}$, and 10 nm , the tip vibration amplitude and minimum height are 60 nm and 0.6 nm , the EM wave of amplitude E_{ext} is coming in at an angle θ (see figure 1) of 60 degrees with respect to the surface normal, we find that $E^s/E_{\text{ext}} = -1.46 + 2.91i$. The finite phase of E^s comes from the radiation resistance of the conical tip. Our calculation directly relates the tip surface field to the incoming external field over the whole cone.

Associated with the tip field of the cone is a tip surface charge density σ_s which radiates at the frequencies modulated by the tapping frequency Ω and eventually leads to the experimental signal. In the experiment, there can be other charges close to the tip. For example, the external EM field induce additional surface charge distribution σ_{element} on the sample surface which is significant for metallic surfaces or when a resonance is excited (such as graphene plasmon) and cannot be simply omitted. The tip charge density σ_s is determined from the condition that the field it generates at the tip, together with that from other charges close to the tip, is equal to the surface field E^s .

In the absence of σ_{element} the sum of the perpendicular components of the displacement fields due to the tip and its image from the sample are continuous so that its change across the interface is zero: $\Delta(D_{\perp, \text{img}} + D_{\perp, \text{tip}}) = 0$. Implicit in this is a surface bound charge $-\nabla \cdot \mathbf{P}$ from the polarization \mathbf{P} induced by the tip charge on the sample surface a distance d away. For finite metallic or resonant elements [2] the external EM field also induces additional spatially varying charges of density σ_{element} on the sample surface. When there are additional charges at the sample surface the boundary condition on the total displacement field D at the surface of the sample is changed to

$$\Delta D_{\perp} = \sigma_{\text{element}}. \quad (2)$$

When σ_{element} is non zero, the total electric field is given by

$$\mathbf{E}_{\text{tot}} = \mathbf{E}_{\text{tip}} + \mathbf{E}_{\text{img}} + \mathbf{E}_{\text{element}} \quad (3)$$

where $\mathbf{E}_{\text{element}}$ is that due to σ_{element} . The total field is the sum of the term due to the tip and its image charges and an additional term due to the surface charge on the element. Since $\Delta D_{\text{element}, \perp} = \sigma_{\text{element}}$, the boundary condition (2) for the total displacement field corresponding to \mathbf{E}_{tot} is obeyed. The fields from the tip-induced charge density $-\nabla \cdot \mathbf{P}$ and that from the external field induced σ_{element} simply add up because

⁴ In practice we have done a two dimensional integral and have calculated a impedance $\mathbf{Z}' = \mathbf{Z}I$.

⁵ The numerical values of these functions recently became available in Mathematica.

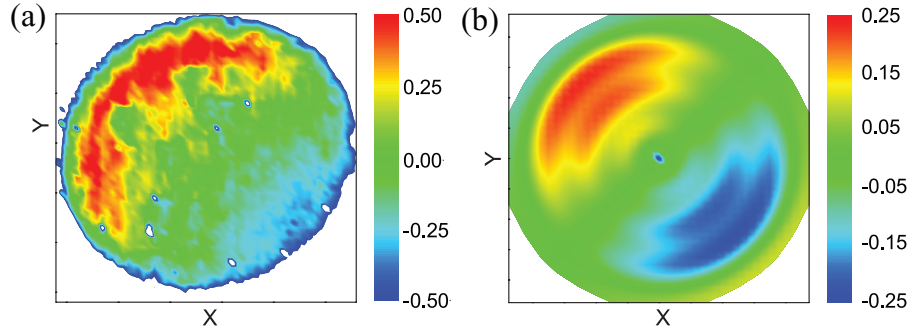


Figure 1. (a) Experimental result for the real part of the amplitude of the two dimensional ‘charge density’ $(S_3 - \langle S_3 \rangle) / \langle S_3 \rangle$ on the disk. (b) Theoretical result for the amplitude of the two dimensional ‘bulk charge density’ $0.12\text{Re}[\sigma^{\text{bulk}}(\mathbf{r})]$ on the disk. The in plane component of the incident field is along the diagonal of this graph.

Maxwell’s equations are linear. The field at the tip is now a sum of a field E_{sa} from a conical surface charge of density σ_s at the tip, a field E_{sb} from the image charge density and now an additional field E_{sc} from charge density σ_{element} :

$$E_s = E_{sa} + E_{sb} + E_{sc}. \quad (4)$$

From Gauss’s law $E_{sa} = \sigma_s / 2\epsilon_0$, $E_{sb} \approx -\beta\sigma_s I(2d) / \epsilon_0$, $\beta\sigma_s$ is the image charge, I is the Coulomb electric field of the image charge⁶. Similarly $E_{sc} = \sigma_{\text{element}} K(d) / \epsilon_0$ ^{7,8}. K is the Coulomb electric field of the element.

In our picture, the boundary electric field E^s is such as to stop the current from going out. Its magnitude is determined by the incoming electromagnetic field averaged over the whole cone. The tip charge density is determined by the requirement that the electric field from it and all other charges close by is equal to the tip field. From equation (4), we get the charge density at the tip given by

$$\sigma_s = [2\epsilon_0 E_s - 2\sigma_{\text{element}} K(d)] / [1 - 2\beta I(2d)]. \quad (5)$$

As the surface charge density of the element is changed, the tip charge density also changes so that the value of E_s is maintained. The tip is vibrating at a frequency Ω so that $d \propto (1 - \cos \Omega t)$. The s-SNOM signal is proportional to the Fourier transform in time of this tip charge density and its image $\beta\sigma_s$ at the n th higher harmonics of the tapping frequency: $S_n \propto (1 + \beta) \int dt e^{i(\omega + n\Omega)t} \sigma_s$. From equation (5) we get

$$S_n = A[B_{0n} - \sigma_{\text{element}} B_{1n} / (2\epsilon_0 E_s)], \quad (6)$$

A is a normalization constant, $B_{1n} = (1 + \beta) \int dt e^{in\Omega t} K(d) / [1 - 2\beta I(2d)]$. $B_{0n} = (1 + \beta) \int dt e^{in\Omega t} / [1 - 2\beta I(2d)]$. The net charge on the disk is zero. Denoting the average over the disk by angular brackets, $\langle \sigma_{\text{element}} \rangle = 0$. Hence $\langle S_n \rangle = AB_{0n}$. From equation (6) we finally obtain

⁶ For elements in the shape of disks $I(x) = \int d\phi \int_0^{R_2} r' dr' r dE_z(r, r', 2x) / (\pi R_2^2)$. $E_z(r) = x[x^2 + r^2 + r'^2 - 2rr' \cos \phi]^{3/2} / (2\pi b^2)$. A factor of 2π from the angular integration is cancelled by a factor of 4π in the denominator from Gauss’ law; the factor of πb^2 is from the averaging normalization.

⁷ $K(x) = \int d\phi \int_0^{R_2} r dr \int_0^{R_{\text{disk}}} \sigma_p(r') r' dr' E_z(r, r', x) / (\pi R_2^2)$. In principle the upper limit of the r' integral for K is $R' = R_{\text{disk}}$. But the large R' contribution is insignificant. We have computed K numerically by doubling R' until it changes by less than one percent.

⁸ The dielectric constant is $\epsilon/\epsilon_0 = 1 - \omega_p^2 / (\omega^2 + i\gamma\omega)$. For Au, $\omega_p = 1.37 \times 10^{16} \text{ rad s}^{-1}$, $\gamma = 4.08 \times 10^{13} \text{ rad s}^{-1}$.

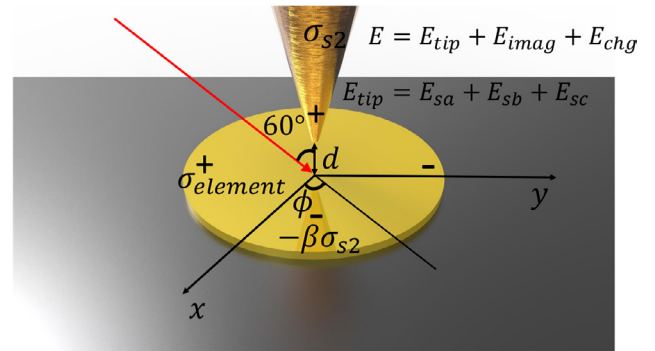


Figure 2. Schematics of the system under study: a metal conic AFM tip is vibrating above a gold disk of radius 530 nm. The system is under monochromatic illumination (red arrow) with a wavelength of $6 \mu\text{m}$ at an angle $\theta = 60^\circ$ with respect to the surface normal. Also shown are the geometric parameters and the composition of the different electric fields, as is defined in the main text.

$$\sigma_{\text{element}} / \sigma_{\text{ext}} = (S_n - \langle S_n \rangle) / \langle S_n \rangle / r_n \quad (7)$$

where $r_n = B_{1n} / B_{0n} / (E_{2s} / E_{\text{ext}})$ is a complex constant only determined by the microscope tip and independent of the samples. $\sigma_{\text{ext}} = \epsilon_0 |\mathbf{E}_{\text{ext}} \times \mathbf{e}_z|$, \mathbf{e}_z is a unit vector normal to the disk. All the spatial dependence of the charge density is contained in $S_n / \langle S_n \rangle - 1$. The phase difference between the experimentally extracted signal and the charge density is independent of the sample.

At the wavelengths of interest (1–10 μm) the dielectric constant ϵ is large and negative, $\beta \approx 1$ and does not change very much. B_{0n} / B_{1n} is relatively constant with a very weak dependence on the frequency. The skin depth $l = [2\rho / (\omega\mu_0)]^{1/2} = 11 \text{ nm}$ is less than the thickness of the disk. We have computed the B s numerically. For $\beta = 1. + 0.011i$ $B_{12} / B_{02} = 0.5464$, $B_{13} / B_{03} = 0.4523$. We thus get for $n = 3$, the proportional factor in equation (7) given by

$$r_2 = -0.075 - 0.15i \quad r_3 = -0.062 - 0.12i. \quad (8)$$

To examine the quantitative values of the charge density in more detail, we show the real part of the charge density extracted from the experimental results along a diagonal in figure 3(a). Also shown is our theoretical result for the real part of the bulk charge density distribution which, in units of

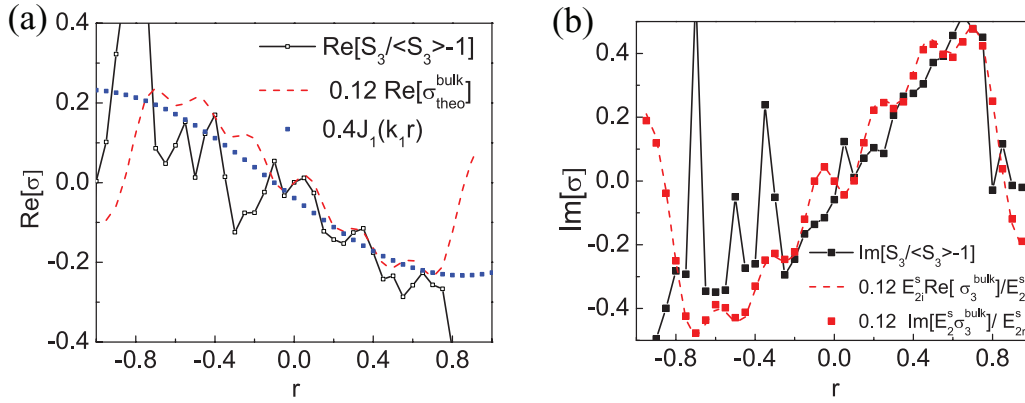


Figure 3. (a) Real part of the ‘charge density’ $(S_3 - \langle S_3 \rangle)/\langle S_3 \rangle$ along a diagonal of the disk (black solid line) and the theoretical estimate for the bulk contribution $0.12\sigma_{\text{bulk}}^{\text{theo}}$ (red dashed line) in units of the $\sigma_{\text{ext}} \sin \theta$. The blue dotted line corresponds to a simple theoretical approximation⁹. (b) Imaginary part of the ‘charge density’ $(S_3 - \langle S_3 \rangle)/\langle S_3 \rangle$ along a diagonal of the disk (black solid line) and the theoretical estimate for the bulk contribution $0.12\text{Im}[r_3 \sigma_{\text{bulk}}^{\text{theo}}]/\text{Re}[r_3]/(\sigma_{\text{ext}})$ (red solid square). Also shown is $0.12\text{Im}[r_3]/\text{Re}[r_3] \sigma_{\text{bulk}}^{\text{theo}}/(\sigma_{\text{ext}})$ (red dashed line). To compare with the experimental measurement, there is very little difference in the results when the imaginary part of the theoretical charge density is not included (lines and symbols) because the theoretical imaginary part is small.

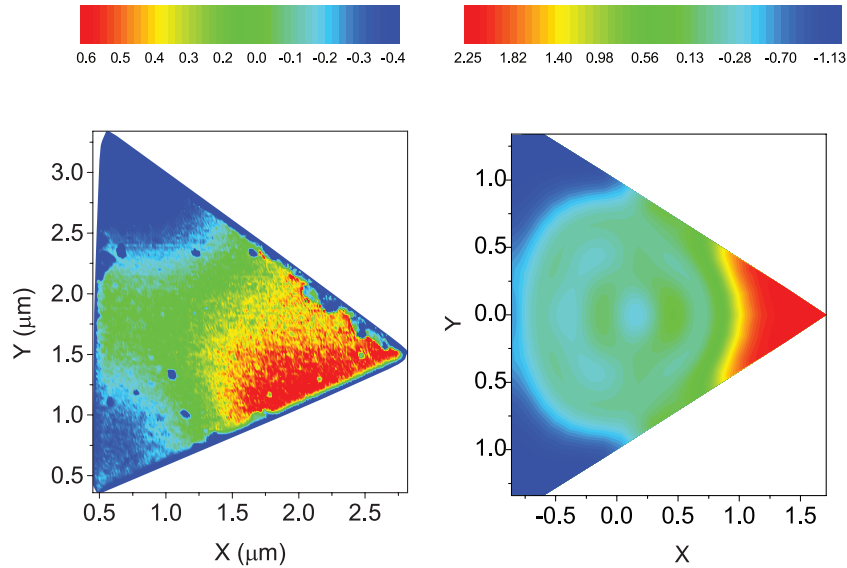


Figure 4. (a) The experimental result of the real part of the two dimensional ‘charge density’ $(S_2 - \langle S_2 \rangle)/\langle S_2 \rangle$ on an approximate equilateral triangle. (b) Theoretical result for the two dimensional ‘bulk charge density’ $0.1\text{Re}[\sigma_{\text{bulk}}^{\text{theo}}(\mathbf{r})]$ on the equilateral triangle. The distance is in arbitrary units. The external field is along the x axis.

σ_{ext} , is close to $(S_3/\langle S_3 \rangle - 1)/0.12$. This is close to our theoretical result in equation (7) (r_3 is evaluated in equation (8)) of $\text{Re}(S_3/\langle S_3 \rangle - 1)/0.124$. Our result suggests that a small variation of the charge density is seen both in theory and experiment and may not be a noise. We also find that the edge charge distribution is $.44\delta(r - R)$. Experimentally $S_3/\langle S_3 \rangle - 1$ exhibit a peak of an approximate area 0.08 at the boundary. Equation (8) suggests that the experimental estimate for the edge term should be $0.16\delta(r - R)$. At the edge, the finite size of the tip creates more error in the interpretation of the experimental data. Our result emphasizes the existence of an edge term, which has not been discussed before.

⁹ We find that [2] the lowest approximation for the radial dependence is $J_1(k_{1D}r)$, where $k_{1D} = 1.84/R$ is determined from the condition that the derivative $J_1'(k_{1D}R) = 0$ at the boundary. This is illustrated by the blue dotted line in this figure.

The comparison between theory and experiment involves a complex numerical constant r_n described in equation (7) which is a function of the AFM tip. The imaginary parts of $S_3/\langle S_3 \rangle - 1$, and $0.12\text{Im}[r_3]/\text{Re}[r_3] \sigma_{\text{bulk}}^{\text{theo}}/\sigma_{\text{ext}}$ along the diagonal direction are shown in figure 3(b). In the region where there is not much fluctuation in the experimental results, the agreement between theory and experiment is good. The phase difference between theory and experiment come from the phase of r_n . In comparing with the experimental measurement, the same multiplication factor for $\sigma_{\text{bulk}}^{\text{theo}}$ is used for both the real and the imaginary parts. There is no adjustable parameter for the phase. We next discuss the example of an equilateral triangle.

With a conformal harmonic mapping (Christofel–Schwarz transformation) between a point $w = x + iy$ in a circle and a point $z = u + iv$ in a triangle so that $dz/dw \propto (1 - w^3)^{-2/3}$,

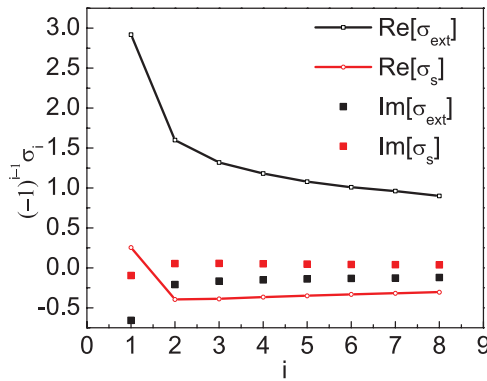


Figure 5. The real and imaginary parts of $(-1)^{j-1}\sigma_j^{\text{ext}}$ and $(-1)^{j-1}\sigma_j^s$ in units of σ_{ext} .



we have recently extended the basis functions and our treatment for the disk to that of triangles [3]. The new basis functions inherited the integrable singularities at the corners from the mapping. With this approach, the charge density induced by an EM field is calculated. In figure 4 we compare the real part of the experimental result and the theoretical charge densities for a gold equilateral triangle with sides of $2.6 \mu\text{m}$ in external electric field with an in plane component along the x axis. Our theoretical calculation for the real part of the bulk charge density distribution in units of σ_{ext} is approximately $(S_2/\langle S_2 \rangle - 1)/0.1$. This is close to our result in equation (7) of $\text{Re}(S_2/\langle S_2 \rangle - 1)/0.15$. For this experimental result the second harmonics with $n = 2$ and not $n = 3$ is used. Experimentally, it is difficult to align perfectly the external field with the symmetry axis of the sample. Aside from this asymmetry, the agreement supports our result in equation (2) that the charge density can be extracted from the s-SNOM data for different n .

We close by discussing the separation of the bulk and the edge contributions for the disk from our numerical solution. The bulk charge contribution is given by $\sigma^{\text{bulk}} = \sigma - \sigma^{\text{edge}}$ where the edge distribution σ^{edge} is a δ function. These functions are all expanded in a Fourier–Bessel series. Consider the general series expansion of a function $s(r)$ in terms of Bessel functions. For $s(r) = \sum_i s_i g_i(r)$ with $g_i = J_m(k_i r)/c_{im}$, the coefficients s_i are given by $s_i = \int r dr s(r) g_i(r)$. We found that higher order terms in the series for σ quickly approaches that for a δ function. If $s(r) = D\delta(r - R)$, $s_i = DRg_i(R)$. For our case, only the $m = 1$ terms are nonzero, $s_i = DRJ_1(k_i R)/c_{1i}$. For large i $s_i = D2^{1/2}(-1)^{i-1}$. In our calculation, the total charge density is a sum of charge densities σ^{ext} and σ^s induced by the electric fields E^{ext} and E^s in equation (1). In figure 5 we plotted the real and imaginary parts of $(-1)^{i-1}\sigma_i^{\text{ext}}$ and $(-1)^{i-1}\sigma_i^s$. For large i , these coefficients all approach constants. From this, we find $\langle(\sigma_i^{\text{ext}} + \sigma_i^s)(-1)^{i-1}\rangle = (-1.29, 0.13)$ where the average is taken over the values for $i = 5, 6, 7, 8$. We thus obtain the edge contribution $\sigma^{\text{edge}}(r) = D\delta(r - R)$ with $D = (-1.29, 0.13)/2^{1/2}$ and the bulk contribution $\sigma_i^{\text{bulk}} = \sigma_i^{\text{ext}} + \sigma_i^s - D(-1)^{i-1}2^{1/2}$.

In summary, we study the charge density distributions in finite metallic structures induced by an EM wave and found

good agreement between theory and experiment. We theoretically prove the normalized near-field scattering signal of s-SNOM $(\langle S_3 \rangle - \langle S_3 \rangle)/\langle S_3 \rangle$ is proportional to the charge density of the metallic structure. In the end, we note that our previous work [25] is ideal for continuous films with intrinsically non-uniform dielectric properties. This work expands the rigorous calculation to subwavelength metal structures with otherwise intrinsically uniform dielectric properties. We have assumed that the intensity of the laser is small enough that there is no significant temperature rise in the sample and thus have not taken this effect into account theoretically. In the future, we will further discuss the data mining of s-SNOM in cases where the samples are highly anisotropic and have strong intrinsic EM resonances.

ORCID iDs

S T Chui  <https://orcid.org/0000-0001-6454-9690>
 Qing Dai  <https://orcid.org/0000-0002-1750-0867>

References

- [1] Alonso-González P *et al* 2017 *Nat. Nanotechnol.* **12** 31–5
- [2] Chui S T, Du J J and Yau S T 2014 *Phys. Rev. E*
- [3] Chui S T, Wang S and Chan C T 2016 *Phys. Rev. E* **E93** 033302
- [4] Novotny L 2007 *Progress in Optics* pp 137–84 (New York: Elsevier)
- [5] Liu M, Sternbach A J and Basov D N 2017 *Rep. Prog. Phys.* **80** 014501
- [6] Hillenbrand R, Taubner T and Keilmann F 2002 *Nature* **418** 159
- [7] Liu M *et al* 2014 *Appl. Phys. Lett.* **104** 1
- [8] Liu M K *et al* 2013 *Phys. Rev. Lett.* **111** 096602
- [9] Qazilbash M M *et al* 2007 *Science* **318** 1750
- [10] McLeod A S *et al* 2016 *Nat. Phys.* **13** 80
- [11] Gilbert Corder S N *et al* 2017 *Phys. Rev. B* **96** 161110
- [12] Gilbert Corder S N *et al* 2017 *Nat. Commun.* **8** 2262
- [13] Post K W *et al* 2018 *Nat. Phys.* **14** 1056–61
- [14] Chen J *et al* 2012 *Nature* **487** 77
- [15] Fei Z *et al* 2012 *Nature* **487** 82
- [16] Xu X G, Tanur A E and Walker G C 2013 *J. Phys. Chem. A* **117** 3348
- [17] Dai S *et al* 2014 *Science* **343** 1125
- [18] Hu F, Luan Y, Scott M E, Yan J, Mandrus D G, Xu X and Fei Z 2017 *Nat. Photon.* **11** 356
- [19] Ni G X *et al* 2018 *Nature* **557** 530
- [20] Alonso-Gonzalez P *et al* 2011 *Nano Lett.* **11** 3922
- [21] Rahmani M, Yoxall E, Hopkins B, Sonnefraud Y, Kivshar Y, Hong M, Phillips C, Maier S A and Miroshnichenko A E 2013 *ACS Nano* **7** 11138
- [22] Hillenbrand R and Keilmann F 2001 *Appl. Phys. B* **73** 239
- [23] García-Etxarri A, Romero I, García de Abajo F J, Hillenbrand R and Aizpurua J 2009 *Phys. Rev. B* **79** 125439
- [24] Chen X, Lo C F B, Zheng W, Hu H, Dai Q and Liu M 2017 *Appl. Phys. Lett.* **111** 223110
- [25] Chui S T, Chen X, Liu M, Lin Z and Zi J 2018 *Phys. Rev. B* **97** 081406
- [26] Chui S T and Zhou L 2013 *Electromagnetic Behaviour of Metallic Wire Structures* (London: Springer)